SFB 609

Sonderforschungsbereich 609
Elektromagnetische Strömungsbeeinflussung in
Metallurgie, Kristallzüchtung und Elektrochemie

M. Hinze, O. Pfeiffer

Active Closed Loop Control Of Weakly Conductive Fluids.

SFB-Preprint SFB609-20-2004

TECHNISCHE UNIVERSITÄT DRESDEN

IFW

mpipks

FZR

BERGAKADEMIE FREIBERG TECHNISCHE UNIVERSITÄT

Preprint Reihe
SFB 609

Diese Arbeit ist mit Unterstützung des von der Deutschen Forschungsgemeinschaft getragenen Sonderforschungsbereiches 609 entstanden und als Manuskript vervielfältigt worden.

Dresden, Oktober 2004

The list of preprints of the Sonderforschungsbereich 609 is available at:
http://www.tu-dresden.de/mwilr/sfb609/pub.html

ACTIVE CLOSED LOOP CONTROL OF WEAKLY CONDUCTIVE FLUIDS

M. HINZE, O. PFEIFFER
TECHNISCHE UNIVERSITÄT DRESDEN
INSTITUT FÜR NUMERISCHE MATHEMATIK
ZELLESCHER WEG 12-14, 01069 DRESDEN
GERMANY

ABSTRACT. The performance of two simple proportional closed-loop control strategies, and of the instantaneous control method in suppressing vortex shedding and drag of the cylinder flow by applying wall near Lorentz forces is discussed. Several numerical results for laminar flow regime are presented.

1. INTRODUCTION

Flow over a bluff body induces drag and lift forces which are undesirable. During the past 100 years there have been many experimental approaches to control the flow around a bluff body in order to reduce drag and increase lift forces and retard separation, e.g. with shaping, blowing/suction, splitter plates, secondary objects and rotation. A comprehensive review can be found in e.g. [5].
In the recent past methods from magneto-hydrodynamics have become a more and more acknowledged in control of conductive fluids by Lorentz forces, cf. [13] and the references cited there.

In this work we present several approaches using Lorentz forces, to suppress the formation of the von Kármán Vortex Street in the cylinder flow, and to decrease drag. We focus on weakly conductive fluids like sea water and other electrolytes. In this case the Lorentz force can be modeled as a near wall body force [4] and the flow is governed by the unsteady incompressible Navier Stokes equations.
As control mechanisms a two-point proportional controller similar to that discussed in [2] and instantaneous control [7] are considered.

2. MATHEMATICAL MODEL

In the present work we consider control of weakly conductive fluids by Lorentz forces. The flow is governed by the unsteady incompressible Navier Stokes equations, and the Lorentz force in this case can be modeled by a near wall distributed force [4], see also the appendix for a derivation. As mathematical model for the velocity vector $y = (y_1, y_2, y_3)$ and the pressure p in the two-dimensional flow domain Ω on the time horizon $[0, T]$ we take

$$
\begin{aligned}
y_t - \nu\Delta y + (y\nabla)y + \nabla p &= F_L \quad \text{in } Q := (0,T)\times\Omega\,, \\
-\nabla\cdot y &= 0 \quad \text{in } Q\,, \\
y(0) &= y^0 \quad \text{in } \Omega,
\end{aligned}
\tag{1}
$$

Date: 29th September 2004.
Key words and phrases. Circular Cylinder, EMHD, proportional controller, Instantaneous Control.

supplied with appropriate boundary conditions. Here the Lorentz force is given by

$$F_L(x) = J_0 B_0 g(\phi) e^{-\frac{\pi}{a}\cdot \text{dist}[x,\text{cylindersurface}]} \vec{t},$$

with

$$g(\phi) = \begin{cases} 1, & \phi_0 \le \phi \le \phi_1 \\ -1, & \pi + \phi_0 \le \phi \le \pi + \phi_1 \\ 0, & \text{else,} \end{cases}$$

and $\vec{t}$ denoting the tangent on the cylinder surface. Here, J_0 denotes the current density, B_0 denotes the magnetic induction at the wall and a is the electrode/magnet spacing, see Fig. 1, where an electrode/magnet arrangement is sketched which produces a tangential Lorentz force. We note, that by altering this arrangement also near wall Lorentz forces can be generated [4].

The Lorentz force F_L enters into the mathematical model (1) as external force. From the

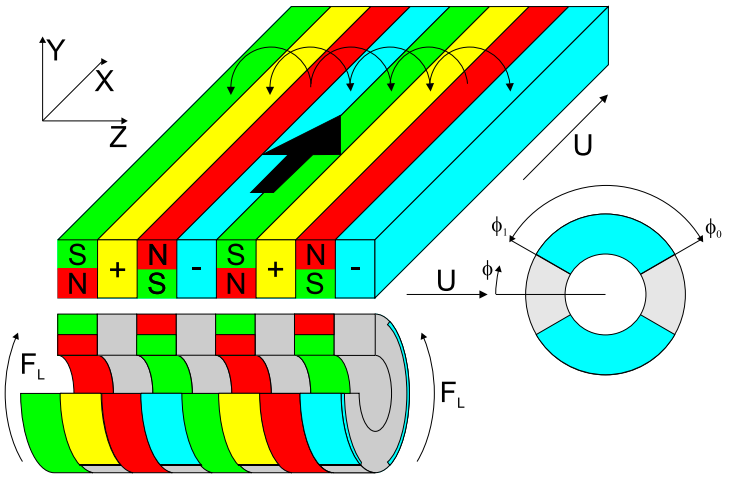

FIGURE 1. Actuator configuration used for computations.

control point of view it may therefore serve as control variable which allows to tailor the flow. In the literature several approaches to flow control with distributed and boundary forces can be found,see [2, 4, 7, 13, 10], and particularly [8] for a comprehensive overview. In the following sections we study control of the cylinder flow by near wall Lorentz forces in the laminar regime (Re < 1000). The flow configuration together with a typical mesh is depicted in Fig. 3. With d denoting the cylinder diameter and U the bulk velocity at the inflow, the Reynolds number is given by

$$\text{Re} = \frac{U\, d}{\nu} \quad ,$$

where ν denotes the constant kinematic viscosity. At the inflow a block profile is prescribed, i.e. $y_1 = U$, $y_2 = 0$, which also is the boundary condition on top and bottom walls. At the cylinder surface no-slip, and at the outflow boundary do-nothing conditions are prescribed. The solution routine is implemented in FEMLAB and validated against the numerical results of [11].

Two physically important parameters are the interaction parameter N, which describes the relation of electromagnetical and inertial forces, and the geometry parameter G. There holds

$$N = \frac{J_0 B_0 d}{\rho U^2} \quad \text{and} \quad G = \frac{a}{d} \quad .$$

In order to compare calculations with different geometry parameters, the so-called scaled interaction parameter $N \cdot G$ is used, compare [11].

The control target consists in reducing the drag force F_D which is composed of the three different parts, i.e.

$$F_D = F_{D_f} + F_{D_p} + F_{D_{em}} \quad ,$$

with

$$F_{D_f} = \int_{\partial \text{cyl.}} \rho\nu\partial_\eta(y\cdot\vec{t})\cdot\eta_2 dS\,, \quad F_{D_p} = -\int_{\partial \text{cyl.}} p\,\eta_1\cdot e_2 dS\,, \quad F_{D_{em}} = -J_0 B_0 \frac{a}{\pi} D(\cos\phi_0 - \cos\phi_1)\,.$$

Here $\eta = (\eta_1, \eta_2)^t$ denotes the outward normal on the cylinder surface. The corresponding drag coefficients are given by

$$C_D = \frac{2F_D}{\rho U^2 D} \quad , \quad C_{D_f} = \frac{2F_{D_f}}{\rho U^2 D} \quad , \quad C_{D_p} = \frac{2F_{D_p}}{\rho U^2 D} \quad , \text{ and } \quad C_{D_{em}} = \frac{2F_{D_{em}}}{\rho U^2 D}$$

with $\rho \equiv 1$ denoting the density. The dependence of drag coefficients on the Reynolds number is depicted in Fig.2.

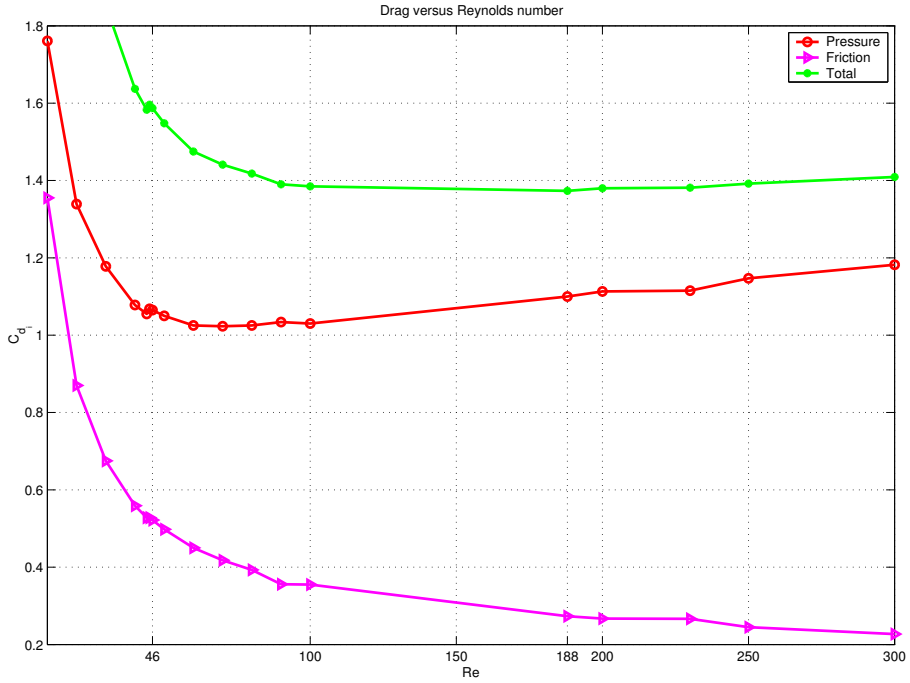

FIGURE 2. Dependency of the drag coefficients on the Reynolds Number.

3. CONSTANT LORENTZ FORCE

In Fig. 4, snapshots of numerical simulations with constant forcing at $T = 10$ are shown. As can be seen the application of a Lorentz force suppresses the vortex shedding. These results are in perfect coincidence with the results reported in [11]. This is illustrated in Fig. 6, where a comparison of the drag coefficients at $\text{Re} = 200$, for $G = 0.5$, and varying N is presented.

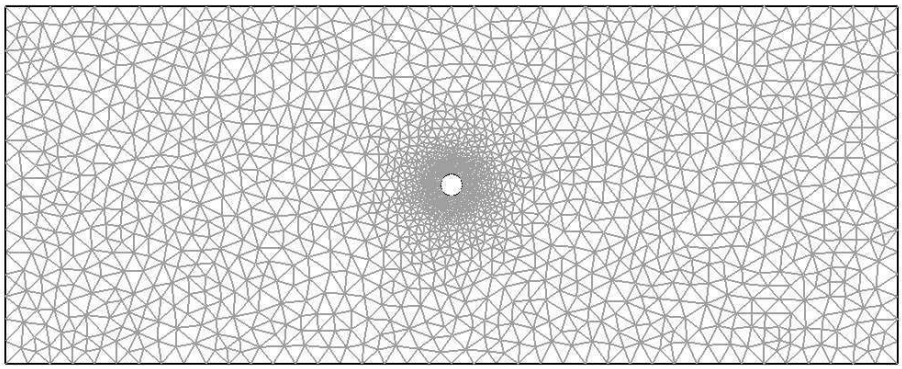

FIGURE 3. Mesh used for computations, consisting of 11.000 elements

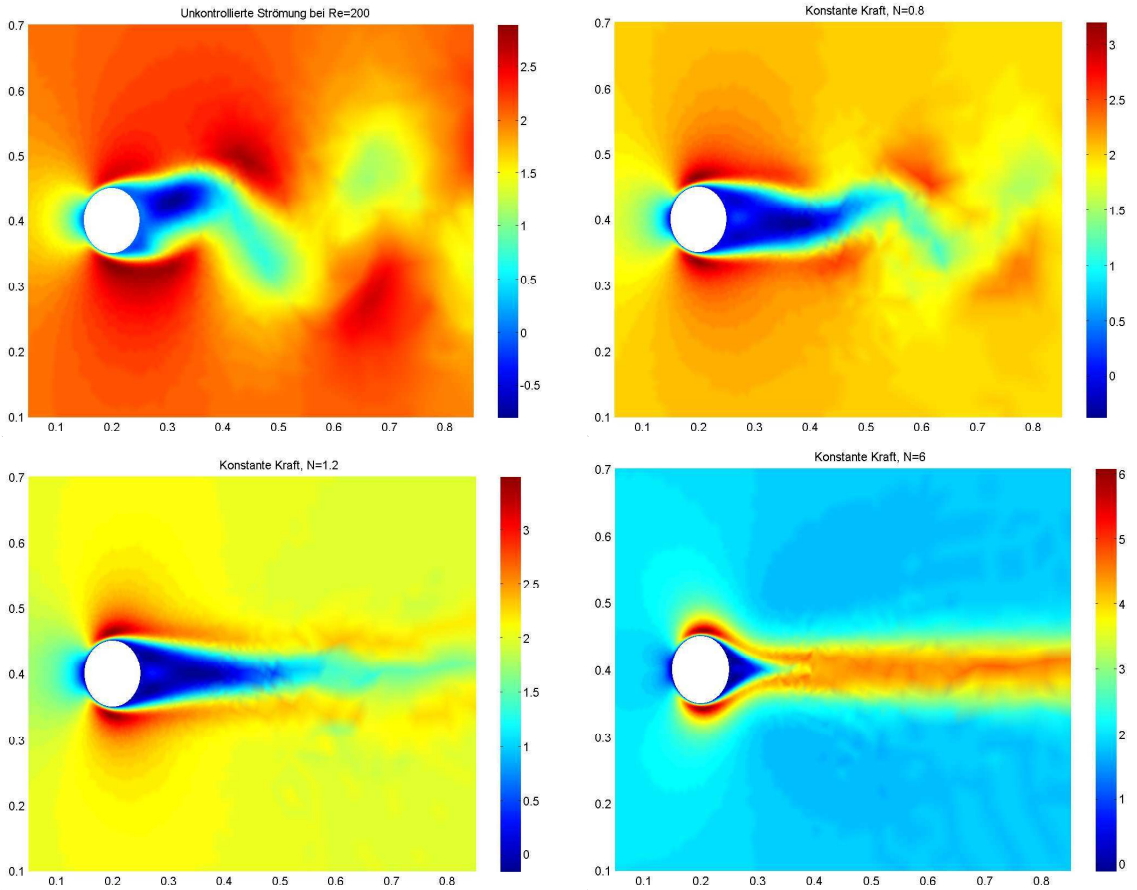

FIGURE 4. Flow velocities for interaction parameters $N = 0$ (without force, top left), 0.8(top right),1.2 (bottom left), and 6 (bottom right)

4. CLOSED LOOP CONTROL

In this section we present two simple closed-loop control strategies which may be regarded as a first step to extend the results of [11] towards fully automatic regulation of flows by near wall Lorentz forces in realistic technical environments. For this purpose two proportional controllers are introduced in the first instance. With regard to experimental realization the following two-point controller will be investigated in detail.

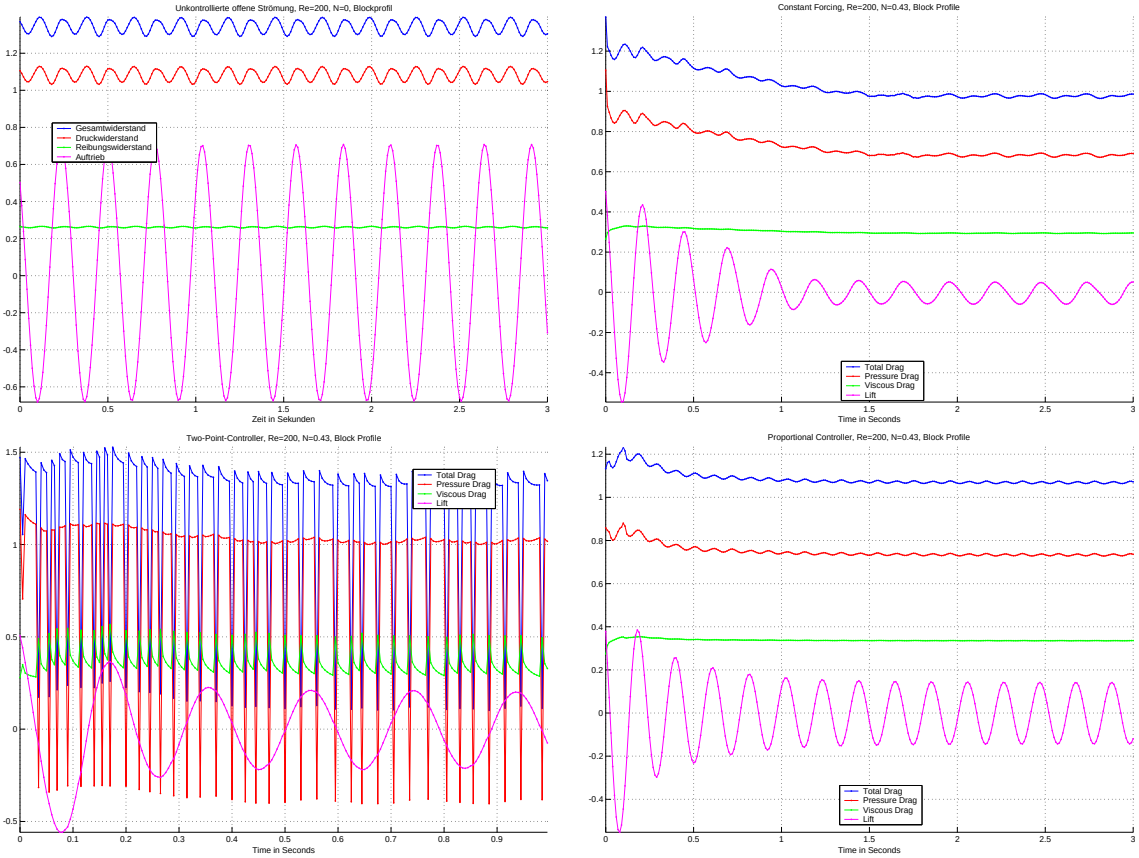

FIGURE 5. Evolution of the drag and lift coefficients at Re=200, uncontrolled case (top left), constant forcing (top right), two-point controller (bottom left), proportional controller (bottom right), in the controlled cases the controller is initialized with on-state at T=0. The interaction parameter then is givenby $N = 0.43$.

Two Point Proportional Controller. The first numerically implemented proportional controller requires that the (signed) flow velocity can be measured at two points in the cylinder wake close to the surface, namely at an angle of $\pm 10^\circ$ behind the rear stagnation point. Whenever upstream flow is detected at one of these two points, the electrodes on the actuators are switched on until the sign of the x_1-component of the flow velocity changes. The design of this controller is inspired by the work of Chen [2]. The interaction parameter N, and thus the Lorentz force at the on-state is constant.

Proportional Controller. The second implemented proportional controller activates whenever a backflow behind the cylinder wall is measured. In contrast to two-point proportional controller the amplitude of the Lorentz force now depends proportionally on the angle where backflow is detected, (see Fig. 11). The closer to the poles backflow is detected, the larger is the amplitude of the Lorentz force, whose maximal value is determined by some a-priorily specified interaction parameter N.

Discussion of the proportional controllers. An energy conservation of up to 20% compared to constant forcing can be achieved with the two-point proportional controller for small interaction parameters ($N \leq 1$), see Fig. 10 (left). This can be explained by the fact that immediately after switching to the on-state the pressure force F_{D_p} decreases significantly. Placement of the measurement points upstream may improve this results,

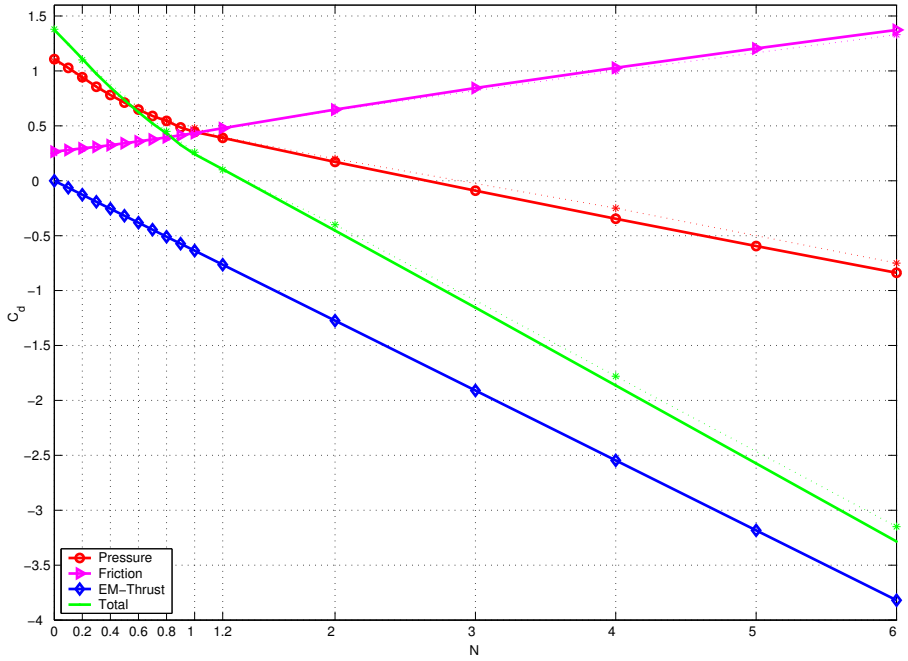

FIGURE 6. Dependency of the drag coefficients on the interaction parameter at Re=200, Comparison with Grundmann/Posdziechs' results.

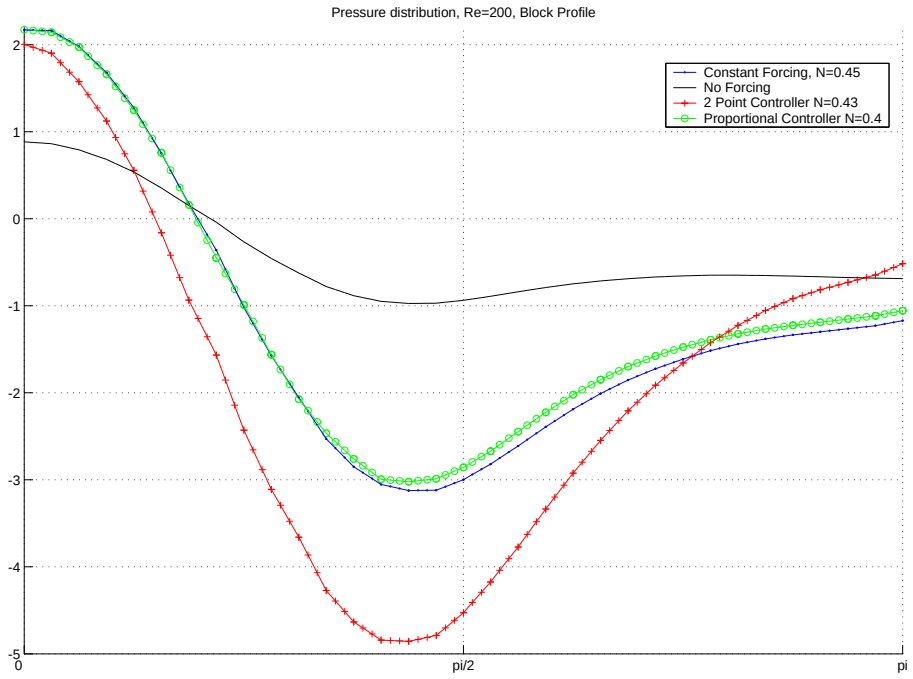

FIGURE 7. Pressure distribution on the cylinder surface from the front to the rear stagnation point: uncontrolled case, constant forcing, two point proportional controller, and proportional controller, N =0.43 in all controlled examples.

as separation is detected earlier. In the thrust region ($N > 1.3$, not represented) the two-point proportional controller supplies no more energy conservation. For small interaction parameters ($N \leq 1$) the proportional controller is not capable of reducing the

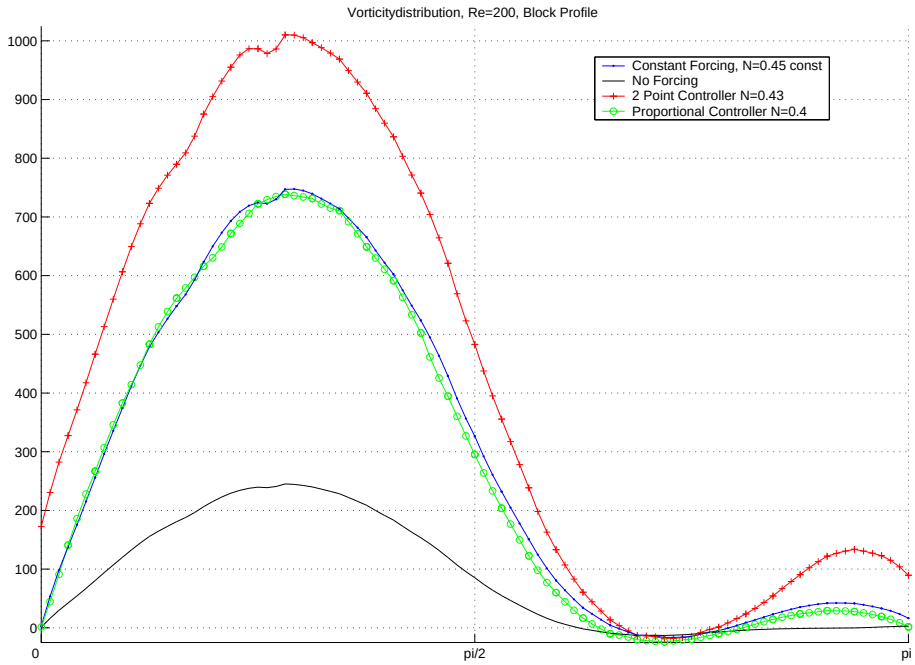

FIGURE 8. Vorticity distribution on the cylinder surface from the front to the rear stagnation point: uncontrolled case, constant forcing, two point proportional controller, and proportional controller, N =0.43 in all controlled examples.

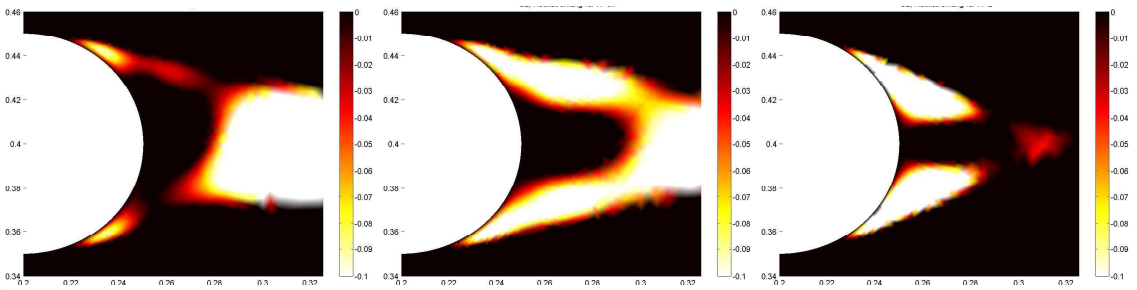

FIGURE 9. View of the upstream flow using the two point proportional controller at different interaction parameters $N = 0.65,\ 2,\ 6$ (left to right, downstream flow regions are represented in black)

total drag coefficient further than constant forcing. For interaction parameters between 1 and 1.7 the proportional controller however achieves up to 8% more drag reduction than constant forcing, see Fig. 10 (right). For even larger values of the interaction parameter the proportional controller is less efficient than constant forcing. Due to these results and since the experimental realization of the proportional controller is much more sophisticated than that for the two-point controller further investigations of the proportional controller are ceased.

In Fig. 8 the vorticity distribution on the surface of the cylinder from the front to the rear stagnation point is represented. It is apparent that in the comparison to the uncontrolled case the vorticity is increased clearly by the application of a Lorentz force. The proportional controllers and constant forcing supply very similar results here. With the two-point controller the largest vorticity is produced.

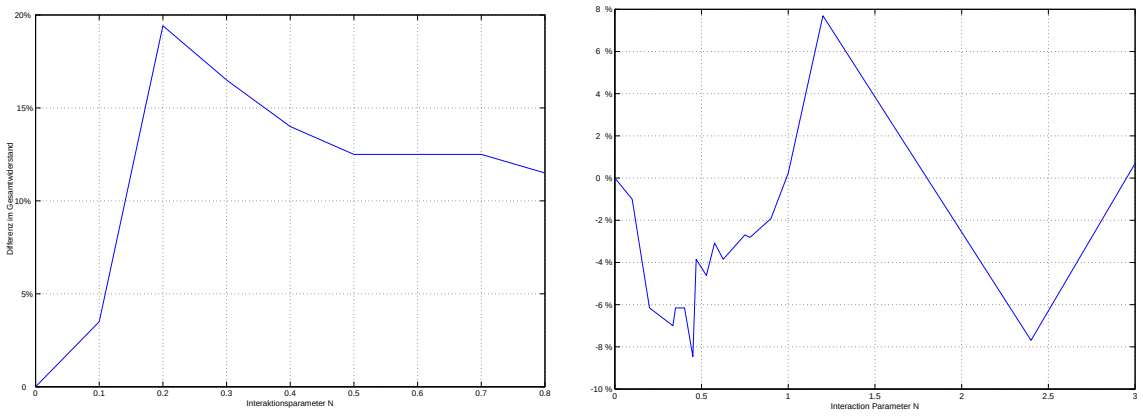

FIGURE 10. Drag reduction won/lost with the controllers (two-point proportional controller on the left, proportional controllers on the right)
.

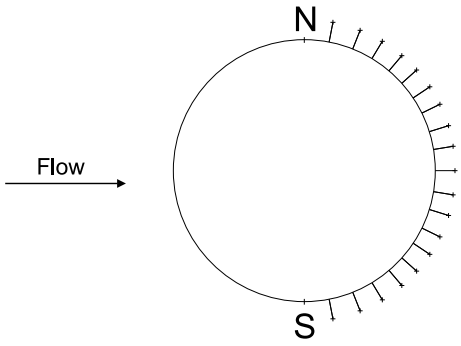

FIGURE 11. Schematic representation of the proportional controller.

The pressure distribution on the cylinder surface is represented in fig. 7. Like for the vorticity distribution the results for the proportional controller and for constant forcing are very similar. The two-point controller obtains the largest pressure reduction. This verifies the results in [2, 3] tendentially.

Finally, we briefly present a mathematical approach to suppress vortex shedding and decrease drag of the cylinder flow, namely instantaneous control. The method allows the interpretation as nonlinear closed-loop control strategy, see [7] for a comprehensive discussion, and all details for the subsequent expositions. In the present situation the method is capable of proposing form and strength of the Lorentz force that should be applied to reach the control goal.

5. INSTANTANEOUS CONTROL

To apply instantaneous control to the cylinder flow we in the present work use the following semi-implicit discretization scheme for the Navier-Stokes system (1) with time step δt: Given y^i, u^{i+1}, find y^{i+1}, p^{i+1} such that

$$e(y^{i+1}, p^{i+1}, u^{i+1}) = 0 \Longleftrightarrow \begin{pmatrix} \frac{1}{\delta t}\mathrm{Id} - \nu\Delta & \nabla \\ -\mathrm{div} & 0 \end{pmatrix} \begin{pmatrix} y^{i+1} \\ p^{i+1} \end{pmatrix} = \begin{pmatrix} r^i \\ 0 \end{pmatrix}, \tag{2}$$

where $r^i := \frac{1}{\delta t} y^i - (y^i \nabla) y^i + (Bu)^{i+1}$, y^{i+1} is supplied with appropriate boundary conditions, and y^0 coincides with the initial condition. Here we have rewritten the Lorentz

force F_L in (1) as

$$F_L(t,x) = (Bu)(t,x) := u(t)g(\phi)e^{-\frac{\pi}{a}dist(x,\text{cylindersurface})}\vec{t},$$

i.e. the term J_0B_0 is replaced by a time-dependent amplitude $u(t)$ which will serve as control input in the control process. We note that (2) for every $r \in L^2(\Omega)^2$ admits a unique solution y, p (superscripts are dropped), so that y as well as p might be considered as functions of the amplitude u. Next we denote by $J(y,p,u)$ some performance measure which allows to relate the control gain (here suppression of vortex shedding and/or drag reduction) to the state variables y, p and to the control action u.

At time instance t^{i+1} we now consider the minimization problem

$$\min \hat{J}(u) := J(y(u),p(u),u) \text{ s.t. } e(y,p,u) = 0. \tag{3}$$

It is well known that the gradient of $\hat{J}(u)$ takes the form

$$\hat{J}'(u) = J_u(y,p,u) - e_u^*(y,p,u)(\lambda,\xi), \tag{4}$$

where (λ,ξ) solves the so called adjoint system

$$e_y^*(y,p,u)(\lambda,\xi) = J_y(y,p,u). \tag{5}$$

Here, * denotes the adjoint of an operator.

The instantaneous control strategy works now as follows. At every time instance t^i, given a control u_o, compute a new control u_n by the steepest descent method, i.e. set

$$u_n = u_o - s\hat{J}'(u_o), \tag{6}$$

where $s > 0$ denotes the gradient step size, and apply u_n to control the system (2). Then proceed to the next time slice and repeat the process.

We now apply this procedure to minimize the friction Force F_{D_f}. As cost functional we therefore choose ($\eta = (\eta_1, \eta_2)$)

$$J(y,p,u) := \int_{\partial cyl} \rho\nu\partial_\eta(y\cdot\vec{t})\eta_2 dS + \frac{\alpha}{2}|u|^2.$$

The first term here measures the quantity of interest, the second term the control cost, were $\alpha > 0$ plays the role of a weight. In this case we have

$$\hat{J}'(u) = \alpha u + B^*\lambda,$$

where (λ,ξ) solves (compare (5))

$$\begin{aligned}
\tfrac{1}{\delta t}\lambda + \nu\Delta\lambda + \nabla\xi &= 0 && \text{in } \Omega,\\
-\text{div } \lambda &= 0 && \text{in } \Omega,\\
\lambda_1 &= \eta_2^2 && \text{on } \partial cyl,\\
\lambda_2 &= -\eta_1\eta_2 && \text{on } \partial cyl,\\
\lambda &= 0 && \text{on } \partial\Omega \setminus (\partial cyl \cup \text{outflow boundary}),\\
\nu\partial_\eta\lambda &= \xi\eta && \text{on outflow boundary},
\end{aligned}$$

and

$$B^*\lambda = \int_\Omega \lambda g(\phi)\vec{t}dx.$$

We note that the adjoint variable λ is independent of y and p and therefore can be computed a-priorily. The update of the control in (6) for $s = \frac{1}{\alpha}$ (which is the optimal step size since the cost functional is linear w.r.t. y and quadratic in u) now reads

$$u_n = \frac{\alpha-1}{\alpha}u_a - \frac{1}{\alpha}\int_\Omega \lambda g(\phi)\vec{t}dx.$$

Finally, we present a numerical example at Re = 100, i.e. $\nu = 0.001$, where we use $\delta t = 0.001$ and apply instantaneous control on the horizon $[0, 4]$, i.e. $T = 4$, with $u_a \equiv 0$, and choose the fully developed vortex street as initial condition y^0. We further set $a = \frac{1}{10}$, so that $G = 1$. The resulting Lorentz force is constant, since $u_n = -\frac{1}{\alpha} \int_\Omega \lambda g(\phi) \vec{t} dx$, and is presented in Fig. 12, right. This amplitude in the present computations corresponds to an interaction parameter of $N = 1.075$. Fig. 12, left shows the evolution of the drag (blue), the friction drag (green) and of the pressure drag (red). Control is switched on at $t = 1$. As can be seen, a drag reduction of approximately 20% is achieved. We note

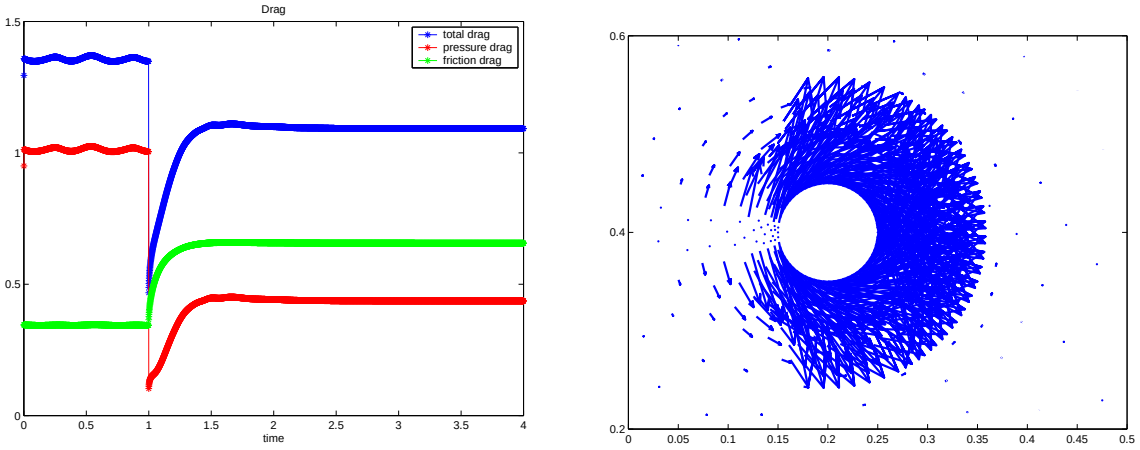

FIGURE 12. Development of drag in instantaneous control (left), and constant Lorentz force resulting from instantaneous control (right).

that the interaction parameter is not a-priorily specified. It results from the optimization approach.

APPENDIX

Simplified Lorentz force, produced by an alternating array of magnets and electrodes. The magnetic flow density vector B and the electrical potential ϕ are determined by Laplace's equation

$$\nabla^2 \phi = 0 \quad , \tag{7}$$

$$\nabla B = 0 \quad , \tag{8}$$

with

$$J = -\sigma \nabla \phi \quad . \tag{9}$$

In order to simplify the solution and produce a force, that does not vary in the flow direction (x), the the magnetic flow density distribution is assumed to be sinusoidal. Again it is assumed that $B_z = 0$, and the induced magnetic field can be neglected. On the surface of the actuator Dirichlet boundary conditions for B and Neumann boundary conditions for ϕ are assumed. The values at the wall ($y = 0$) are thus

$$J_y|_{\text{wall}} = J_0 \sin(\frac{\pi}{2a} x) = -\sigma \frac{\partial \phi}{\partial y}|_{\text{wall}} \quad , \tag{10}$$

$$B_y|_{\text{wall}} = B_0 \cos(\frac{\pi}{2a} x) \quad . \tag{11}$$

The domain (7)-(9) is a channel with height of 2δ with insulating upper wall (i.e. $B_{y=2\delta}|_{\text{wall}} = 0$, and $J_{y=2\delta}|_{\text{wall}} = 0$. The current density and flow density distributions are

$$J_x(x,y) = -\frac{J_0}{\tanh(\frac{\pi}{a}\delta)}\cos(\frac{\pi}{2a}x)[-\tanh(\frac{\pi}{a}\delta)\sinh(\frac{\pi}{2a}y)] \quad , \tag{12}$$

$$J_y(x,y) = -\frac{J_0}{\tanh(\frac{\pi}{a}\delta)}\sin(\frac{\pi}{2a}x)[-\tanh(\frac{\pi}{a}\delta)\cosh(\frac{\pi}{2a}y)] \quad , \tag{13}$$

$$B_x(x,y) = -B_0\sin(\frac{\pi}{2a}x)[\sinh(\frac{\pi}{2a}y) - \frac{\cosh(\frac{\pi}{2a}y)}{\tanh(\frac{\pi}{2a}\delta)}] \quad , \tag{14}$$

$$B_y(x,y) = -B_0\cos(\frac{\pi}{2a}x)[\cosh(\frac{\pi}{2a}y) - \frac{\sinh(\frac{\pi}{2a}y)}{\tanh(\frac{\pi}{2a}\delta)}] \quad . \tag{15}$$

By taking the cross product of the current density and the magnetic flow density the resulting strength acts in x direction only, is thus a function of the wall-normal distance y only

$$f_z = J_0B_0[\sinh(\frac{\pi}{2a}y) - \frac{\cosh(\frac{\pi}{2a}y)}{\tanh(\frac{\pi}{2a}\delta)}] \times [\cosh(\frac{\pi}{2a}y) - \frac{\sinh(\frac{\pi}{2a}y)}{\tanh(\frac{\pi}{2a}\delta)}] \quad . \tag{16}$$

For $\frac{\delta}{a} \to \infty$

$$f_i = \delta_{i3}J_0B_0\exp(-\frac{\pi}{a}y) \quad . \tag{17}$$

REFERENCES

[1] K. Afanasiev: Stabilitätsanalyse, niedrigdimensionale Modellierung und optimale Kontrolle der Kreiszylinderumströmung, Dissertation, TU Dresden 2001

[2] Z. Chen: *Electro-Magnetic Control of Cylinder Wake*, Dissertation,New Jersey Institute of Technology, May 2001

[3] Z. Chen, N. Aubry: Communications in Nonlinear Science and Numerical Simulation, 2003

[4] T. Berger, J. Kim, C. Lee, J. Lim: *Turbulent boundary layer control utilizing the Lorentz force*, Physics of Fluids, Vol 12 #3, March 2000, pp. 631-649

[5] M. Gad-el-Hak: *Modern Developments in Flow Control*. In: Appl. Mech. Rev. 49 (1996), pp365-379

[6] R.D. Henderson: *Details of the drag curve near the onset of vortex shedding*, Aeronautics and Applied Mathematics, California Institute of Technology, pp. 2102-2104, 1995

[7] M. Hinze: *Optimal and instantaneous control of the instationary Navier-Stokes equations*, Habilitation thesis (2000), Fachbereich Mathematik, Technische Universität Berlin.

[8] M.D. Gunzburger, *Perspectives of flow control and Optimization*, Siam, 2003

[9] P. Poncet: Phys. Fluids 14, 2021-2023, 2002

[10] P. Poncet, P. Koumoutsakos: Proceedings of The Fourteenth International OFFSHORE AND POLAR ENGINEERING CONFERENCE, 2004

[11] O. Posdziech, R. Grundmann: *Electromagnetic control of seawater flow around circular cylinders*, Eur. J. Mech. B - Fluids 20, 2001, pp. 255-274

[12] T. Weier, Fey, G. Gerbeth, G. Mutschke, G. Avilov: *Boundary layer control by means of electromagnetic forces*. ERCOFTAC Bulletin 44 2000, pp.36-40

[13] T. Weier, G. Gerbeth, G. Mutschke, O. Lielausis, G. Lammers: *Control of Flow Separation Using Electromagnetic Forces*, SFB 609 Preprint 2004-03

[14] T. Weier, J. Fey, G. Gerbeth, G. Mutschke, O. Lielausis, G. Platacis: *Boundary layer control by means of wall parallel Lorentz forces*. Magnetohydrodynamics . 2001. Vol. 37, No. 1/2, pp. 177-186

[15] T. Weier, G. Gerbeth, G. Mutschke, G. Platacis, O. Lielausis: *Experiments on cylinder wake stabilization in an electrolyte solution by means of electromagnetic forces localized on the cylinder surface*. Experimental Thermal and Fluid Science 16 (1998), pp.84-91

E-mail address: `hinze@math.tu-dresden.de,pfeiffer@math.tu-berlin.de`

URL: `http://www.math.tu-dresden.de/~hinze`